Synchronous Power Controller With Flexible Droop Characteristics for Renewable Power Generation Systems

Weiyi Zhang, *Student Member, IEEE*, Antoni Mir Cantarellas, *Student Member, IEEE*, Joan Rocabert, *Member, IEEE*, Alvaro Luna, *Member, IEEE*, and Pedro Rodriguez, *Fellow, IEEE*

***Abstract*—The increasing amount of renewable power generation systems is a challenging issue for the control and operation of the electrical networks. One of the main issues is their lack of inertia, which is becoming a greater problem as much as the share of the power plants based on traditional synchronous generators gets reduced. In this regard, the new grid codes ask these plants to provide new functionalities such as the frequency support and inertia emulation. In this paper, a synchronous power controller for grid-connected converters is proposed as a good solution for the renewable generation systems with energy storage. It provides inertia, damping, and flexible droop characteristics. Different from the faithful replication of the swing equation of synchronous machines, an alternative control structure is proposed, by which the damping and inherent droop slope can be configured independently to meet the requirements in both dynamics and frequency regulations. Analysis and experimental results are both shown to validate the proposed controller.**

***Index Terms*—DC–AC power conversion, inertia emulation, power generation control, synchronous power controller.**

I. Introduction

TRADITIONAL generation plants based on renewable energy sources (RES) act as grid-feeding systems, which deliver the maximum power from the primary source to the grid [1]. As much as the penetration of the RES generation plants increases, the insufficient inertia in the whole network could undermine its operating stability. Therefore, the control objectives and dynamics of the grid-connected converters need to be adjusted to take more responsibilities in grid supporting issues, like as inertia emulation, frequency regulation and voltage support.

The droop control strategy has been implemented in the control of grid-connected converters as seen in [2]–[6]. Even though the outer droop loops allow the grid-connected converters to adjust the steady-state power injection according to the demand of the grid, the transient behaviors of these converters are not good enough. The lack of inertia is still a drawback, which cannot be improved by droop control without jeopardizing the stable operation of a grid-connected converter.

A solution to improve the dynamics of the converters is to specify the properties of the grid-connected converters in such a way that it acts like a synchronous generator (SG), as is proposed in [7]. It is an approach that has been drawing a lot of interests in the recent years. This trend is initiated by the fact that conventional grid synchronization algorithm like Phase-locked loop (PLL) presents not inertia characteristics, and the dynamics of any supporting strategy is affected by the inherent dynamics of the PLL. Moreover, a PLL might have a negative impact on the control performance under weak ac grids [8].

A control implementation scheme for the emulation of SG is proposed in [9], in which the loop filter of the conventional PLL is modified to emulate the inertia and damping characteristics. Other similar design or proposals incorporating inertia and damping in a PLL can be found in [10] and [11]. Based on the strategy in [9]–[11], the inertia effect is only linked to the grid frequency, and does not essentially exist while reacting to the power input variations. Then the perturbations in the dc side will be directly transmitted to the ac side without inertia. In addition, the inertia effect does not exist in island operation based on this type of design.

Another implementation strategy for emulating SG is proposed and analyzed in [8], in which the PLL is substituted by an active power synchronization loop. Even though this strategy has shown advantages in the interconnection of weak ac grids [12], the inertia and oscillation damping are not specifically addressed, and it has to be switched to a PLL-based vector current control under severe ac faults.

In [13]–[15], a torque synchronization loop is designed considering inertia and damping characteristics. A similar strategy is also adopted in [16]. The authors in [17]–[19] propose a synchronous power controller presenting inertia and damping characteristics, and particularly a virtual admittance structure is proposed. The authors in [20] and [21] indicate that the inertia can also be implemented in the microgrid droop controller, making use of the first-order low-pass filter which is traditionally used only for damping the measurement noise.

The abovementioned designs in [13]–[21] incorporate the swing equation inherently in the power regulating loop, thus

Manuscript received September 10, 2015; revised January 2, 2016 and March 4, 2016; accepted April 25, 2016. Date of publication May 16, 2016; date of current version October 7, 2016. This work was supported in part by the Spanish Ministry of Economy and Competitiveness under the Project ENE2014-60228-R. Paper no. TSTE-00763-2015.

W. Zhang, J. Rocabert, and A. Luna are with the Department of Electrical Engineering, Technical University of Catalonia, Barcelona 08222, Spain (e-mail: weiyi.zhang@estudiant.upc.edu; rocabert@ee.upc.edu; luna@ee.upc.edu).

A. M. Cantarellas and P. Rodriguez are with the Department of Electrical Engineering, Technical University of Catalonia, Barcelona 08222, Spain, and also with the Abengoa Research, Seville 41014, Spain (e-mail: antoni.mir@abengoa.com; pedro.rodriguez@abengoa.com).

Color versions of one or more of the figures in this paper are available online at http://ieeexplore.ieee.org.

Digital Object Identifier 10.1109/TSTE.2016.2565059

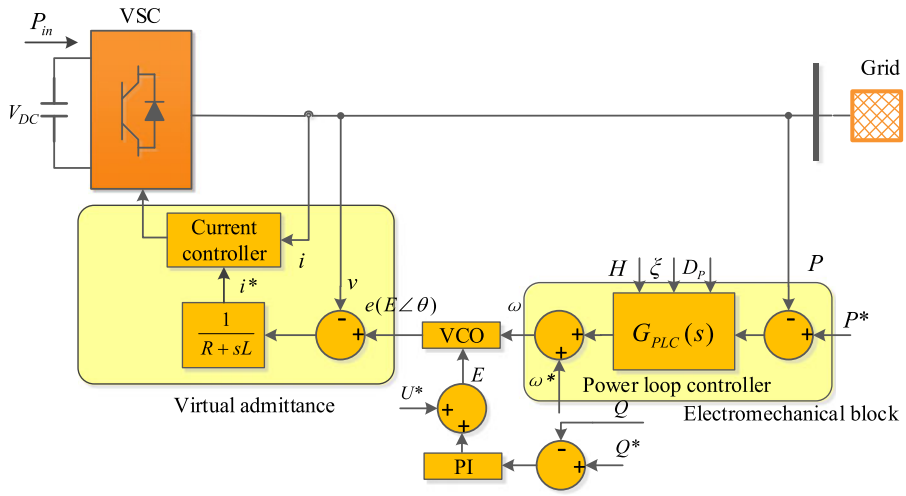

Fig. 1. The overall control scheme of synchronous power controller.

the power synchronizing effect will be present in both grid-connected or island operation. Nevertheless, the damping effect and the power–frequency droop slope are constrained by each other. Due to this, a good parameter for the droop feature may lead to an insufficient damping, and in the other way around, a proper damping parameter could give rise to an undesired droop slope. On the other hand, since the droop characteristics is naturally incorporated in the power regulating loop, a fixed power control cannot be directly achieved even if it is needed in some applications. In [13], the authors propose to use an additional PI controller with a virtual switch to adjust the damping channel to achieve a fixed power control if needed, but the order of the closed-loop transfer function will increase, thus the dynamic analysis and tuning of parameters become more complex.

This paper proposes a synchronous power controller with inertia, damping and flexible droop characteristics for grid-connected converters. Compared with the existing techniques, damping and droop characteristics are particularly addressed, while the inertia feature is maintained. The damping performance is important for the local stability and dynamics of the RES-based generation systems. And the droop characteristics is necessary to fulfil the required frequency support. Therefore, instead of tuning a single parameter to find a good tradeoff between both damping and droop characteristics, a power loop controller is proposed to configure damping and droop characteristics separately. In addition, an explicit relation among the controller gains, inertia, damping coefficient and droop slope is given, and thus the proposed method makes a flexible control paradigm possible in which the controller gains can be adaptive.

The remaining part of the paper is organized as follows. In Section II, the mechanism and implementation of the overall architecture of the synchronous power controller is introduced briefly. In Section III, the design of the electromechanical block is presented and a power loop controller is proposed. The control parameters setting is shown in Section IV. Finally, in Section V and VI, simulation and experimental results are respectively given.

II. Overall Control Structure

The proposed power loop controller is based on the general synchronous power control (SPC) architecture shown in Fig. 1. This control scheme is mainly characterized by two blocks, the electromechanical block and the virtual admittance block, which are respectively described in [17], [22], [23]. In addition to the control scheme shown in Fig. 1, outer loops can be added. Depending on the requirements of the grid and the configuration and control strategy at the dc side, the outer loops can vary. Normally a *Q-V* droop controller is added for weak grid support and island grid forming. And considering the limited power reserve from the dc side, an outer $P-V_{\rm dc}$ droop control can also be included as an addition to the *P-f* characteristics.

Based on the general control structure, the inertia can be essentially incorporated in the electromechanical control loop by properly designing the power loop controller.

As shown in Fig. 1, the power loop controller generates a virtual synchronous frequency ω, which is then integrated to a phase signal θ. Combining the phase signal θ and the magnitude signal E (generated by the reactive power controller), the virtual electromotive force e will be generated by the voltage controlled oscillator (VCO). In this case a PI controller is implemented in the reactive power control loop.

The virtual admittance structure adopted in [13], [18] is selected as the structure of the inner control loops, which is shown in Fig. 2. It is an emulation of the output impedance of SG. This block plays a key role in load sharing and presents a natural voltage magnitude droop feature for grid voltage support.

Compared with the well-known virtual impedance structure, the virtual admittance structure emulates the output impedance without leading to the difficulties in implementation. The main advantages lay on the effectiveness for the complete range of harmonic frequencies and the simplicity in the inner loop implementation [18].

According to the electrical characteristics of the synchronous machines, the generated active power can be approximated to (1), considering that the output impedance of SG is mainly

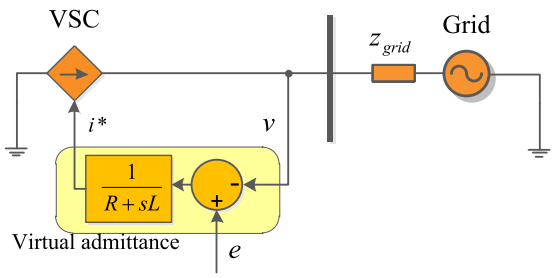

Fig. 2. Virtual admittance emulating the electrical characteristics of synchronous machines.

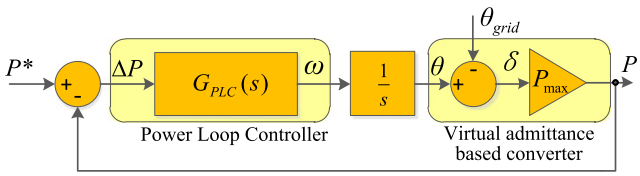

Fig. 3. Modeling of active power control loop.

inductive.

$$\Delta P = P_{\max}\Delta\delta \tag{1}$$

where ΔP is the incremental generated power, and $\Delta\delta$ is the incremental phase-angle difference between the virtual electromotive force e and the grid voltage v in each phase. The admittance gain is expressed as,

$$P_{\max} = \frac{EV}{X} \tag{2}$$

where E and V are respectively the rms values of e and v, and X the value of the reactance provided by the virtual admittance.

Based on (1), the inner control loops can be simply modeled as an admittance gain since it has much faster dynamics compared with outer loops. So it avoids the complexity in the analysis of power loop.

III. Electromechanical Block

According to the control scheme shown in Fig. 1, the active power regulating loop can be modeled as shown in Fig. 3, where the power loop controller $G_{\rm PLC}(s)$ is designed in this section. The synchronization mechanism of the SPC-based converter is similar to the one of a SG. Even if the grid voltage angle $\theta_{\rm grid}$ is unknown, the synchronous angular speed ω can always be adjusted to accordingly shift the load angle δ. In this way the active power is regulated.

As the main focus of this paper, a power loop controller is proposed. In the following, the existing techniques that virtually implement the swing equation of SG are analyzed first, and the boundaries of the existing techniques are shown. Then an alternative controller is proposed, and the mathematical relationship between the characteristic parameters and the control parameters is illustrated.

A. Mechanical Power Loop (MPL) Controller

The SG swing equation can be expressed as (3) in terms of power, for small signals of the rotor angular frequency ω around the synchronous frequency.

$$P_{\rm mech} - P_{\rm elec} = \omega_s(Js + D)\omega. \tag{3}$$

In (3), $P_{\rm mech}$ is the input mechanical power, $P_{\rm elec}$ the output electrical power, ω_s the synchronous angular frequency, J the moment of inertia and D the damping parameter. Even though the damper winding of SG can provide the damping effect, it is relatively limited. Considering this fact, the damping of the power loop can be improved and optimized for control of grid-connected converters. Therefore, the damping term is considered as well as the inertia.

Based on the swing equation, the form of $G_{\rm PLC}(s)$ can be designed as shown in (4), which is referenced as MPL controller in this paper

$$G_{\rm PLC}(s) = \frac{1}{\omega_s(Js + D)}. \tag{4}$$

According to (4), the resulting closed-loop transfer function is obtained and shown in

$$\frac{P}{P^*}(s) = \frac{{\omega_n}^2}{s^2 + 2\xi\omega_n s + {\omega_n}^2} \tag{5a}$$

$$\xi = \frac{D}{2}\sqrt{\frac{\omega_s}{JP_{\max}}} \tag{5b}$$

$$\omega_n = \sqrt{\frac{P_{\max}}{J\omega_s}}. \tag{5c}$$

Equation (5a) is given in the specific form as an analogy of the second order parametric transfer function, for which the time response is defined by the parameters ω_n and ξ. Moreover, ω_n and ξ are also linked to the damping and inertia parameters of the SG swing equation through (5b) and (5c).

To guarantee the local stability of the system, ξ has to be specified greater than zero.

Instead of using the moment of inertia J to designate the inertia characteristics, the inertia constant H is commonly adopted, which is defined in (6), meaning the time it takes to accelerate the rotational speed from zero to ω_s using full power S_N [24]

$$H = \frac{J{\omega_s}^2}{2S_N}. \tag{6}$$

For analyzing the dynamics of the power control loop, the response to frequency disturbances also needs to be studied. In the modeling, the grid frequency can be linked to the grid phase angle by an integrator. According to Fig. 3, taking ω_g as the variable while taking P as the function, the associated transfer function (P-f response) is shown in (7).

$$\frac{\Delta P}{\Delta\omega_g}(s) = \frac{-P_{\max}(s + 2\xi\omega_n)}{s^2 + 2\xi\omega_n s + {\omega_n}^2}. \tag{7}$$

It is seen from (7) that the MPL controller incorporates an intrinsic P-f droop feature. If the droop ratio D_P is defined as (8), which describes the steady-state power variation caused by

the grid frequency change,

$$D_P = \left(\frac{2\pi}{1000}\right) \cdot \left|\frac{\Delta P}{\Delta \omega_g}(0)\right| \text{kW/hz} \tag{8}$$

then combining (7) and (8), the intrinsic droop ratio of the MPL controller $D_{P(\text{MPL})}$ is expressed in

$$D_{P(\text{MPL})} = \frac{4\pi\xi P_{\max}}{1000\omega_n}. \tag{9}$$

It is seen that the MPL controller brings about a continuous power synchronizing behavior as long as the grid frequency deviates from the nominal value. However, the droop ratio D_P is constrained by the inertia and damping parameters that leads to a tradeoff in the parameters setting.

B. Boundaries of the MPL Controller

To further show the restrictions of the MPL controller in parameters tuning, the grid frequency deviation percentage that extracts the full rated power from the converter is used as the indicator of the droop characteristics, which is represented by *1/R* [25]. The relation between D_P and *1/R* is shown in

$$\frac{1}{R} = \frac{2\pi S_N}{D_P \omega_s}. \tag{10}$$

Then the interaction among inertia, damping and droop slope defined by the MPL controller is obtained as written in (11), which is derived combining (5c), (6), (9) and (10)

$$\frac{1}{R}(\text{MPL}) = \frac{1}{2\xi}\sqrt{\frac{X_{pu}}{2H\omega_s}} \tag{11}$$

where X_{pu} represents the per-unit value of the reactance of virtual admittance and is expressed in

$$X_{\text{pu}} = \frac{S_N}{P_{\max}}. \tag{12}$$

Equation (11) shows the interaction among H, ξ, X_{pu} and *1/R*. And since the values of H and X_{pu} can be pre-fixed respectively considering the design requirement, the challenge mainly lies in the restriction between ξ and *1/R*.

This restriction is visualized in Fig. 4, where H is specified to 2, 11 and 20 respectively in three cases. The grid nominal frequency is set to 50 Hz and X_{pu} is set to 0.3 to specify the model.

As shown in Fig. 4, once the damping coefficient ξ is tuned and fixed, the droop slope will be fixed, too. However on the other hand, the droop slope needs to be specified considering the frequency variation of the utility grid and the power reserve of the generation plants.

For traditional SGs, a typical range of droop slope is $4\% < 1/R < 5\%$ [25]. But for RES-based generation plants, *1/R* may have to be greater taking into account the power reserve that is technically and economically feasible. In the scenarios shown in Fig. 4, *1/R* is below 3%. If *1/R* is required to be greater, ξ has to be reduced, which undermines the damping performance.

This issue will not exist if the grid is dominated by the converters controlled with the MPL controllers, since a small value of *1/R* leads to stronger effect in opposing frequency deviation. However, if the total generation is dominated by traditional synchronous generators, the frequency variation in the grid can cause frequent saturation or low power quality injection of the generation units that have a small value of *1/R*.

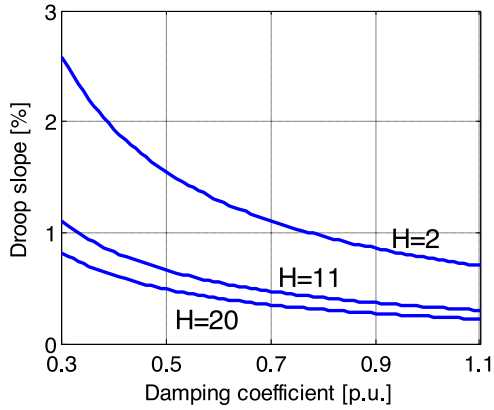

Fig. 4. The relation between the droop slope *1/R* and the damping coefficient ξ.

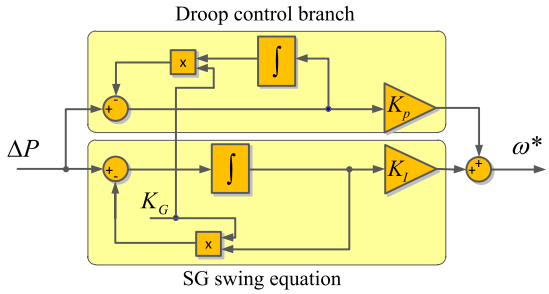

Fig. 5. The proposed power loop controller.

C. Configurable Natural Droop (CND) Controller

In order to achieve a good grid interactive performance in which the droop slope can be specified independent of the damping parameter, a power loop controller with inertia, damping and flexible droop characteristics is proposed as shown in Fig. 5.

Other than the implementation of the swing equation of an SG, a droop branch is included in parallel for controlling the *P-f* droop slope in steady state. In this way it adjusts the offset of the power transfer function by introducing a new degree of freedom. The structure of the droop branch is developed in the way that it shares the same denominator with the transfer function of the swing equation. In this manner the order of the power regulating loop does not increase. In a practical implementation the integrators in the controller can be discretized using the Tustin trapezoidal method for an accurate equivalence.

The transfer function of the proposed controller is generalized as written in (13), which is referred as CND controller in this paper

$$G_{\text{PLC}}(s) = \frac{K_P s + K_I}{s + K_G}. \tag{13}$$

Compared with the MPL controller, the CND controller provides an additional degree of freedom without increasing the order of the power regulating transfer function. And it gives a natural *P-f* droop feature which can be configured independent to the inertia and damping parameters.

Substituting the power loop controller block in Fig. 3 with the expression (13), the resulting closed loop transfer function is shown in (14a). The damping coefficient and natural frequency are respectively expressed in (14b) and (14c)

$$\frac{P}{P^*}(s) = \frac{(2\xi\omega_n - K_G)s + \omega_n^2}{s^2 + 2\xi\omega_n s + \omega_n^2} \tag{14a}$$

$$\xi = \frac{P_{\max}K_P + K_G}{2\omega_n} \tag{14b}$$

$$\omega_n = \sqrt{P_{\max}K_I}. \tag{14c}$$

Even though (14a) has a different expression in the numerator compared with the standard second-order parametric transfer function, the denominator of the system is the same. Therefore, in order to place the closed-loop poles in the left half plain to guarantee the stability, ξ still has to be specified greater than zero.

The *P-f* response of the CND controller is shown in,

$$\frac{\Delta P}{\Delta\omega_g}(s) = \frac{-P_{\max}(s + K_G)}{s^2 + 2\xi\omega_n s + \omega_n^2} \tag{15}$$

where (16) is obtained.

$$D_{P(\mathrm{CND})} = \frac{2\pi K_G}{1000K_I}. \tag{16}$$

According to (14b), (14c) and (16), by specifying the control parameters K_P, K_I and K_G, the inertia, damping and droop characteristics can be respectively given. Besides, the natural frequency ω_n can be translated to the inertia constant H by combining (5c) and (14c) to equate the ω_n from two cases. Optionally, D_P can be set to zero if the plant is assigned to have a fixed power control.

IV. Control Parameters Setting

The control parameters K_P, K_I and K_G can be clearly set according to the input of D_P, H and ξ. Owing to the explicit link between the controller gains and characteristic parameters, the controller can easily be made adaptive according to the secondary control, and a flexible control paradigm becomes possible. In the implementation the algorithm for calculating the control parameters based on (14b), (14c) and (16) can be embedded in the converter controller, but will only be activated when the secondary commands are updated.

As mentioned in the former section, D_P is the droop ratio that needs to be determined based on the frequency variation of the utility grid and the feasible power reserve. H can be designated considering the inertia constant of the SG that has the same power level. And the damping coefficient ξ can be set considering the typical value range $0 < \xi < 1$ to create a stable and under-damped system.

In order to further tune ξ, the analysis on dynamics is done based on the mathematical transfer functions given in the former section. A unitary step input is given to the closed loop transfer function (14a), and the influence of ξ on the settling time and overshoot of the time response can be calculated. Then ξ can be adjusted to meet the requirements of the converter and the grid.

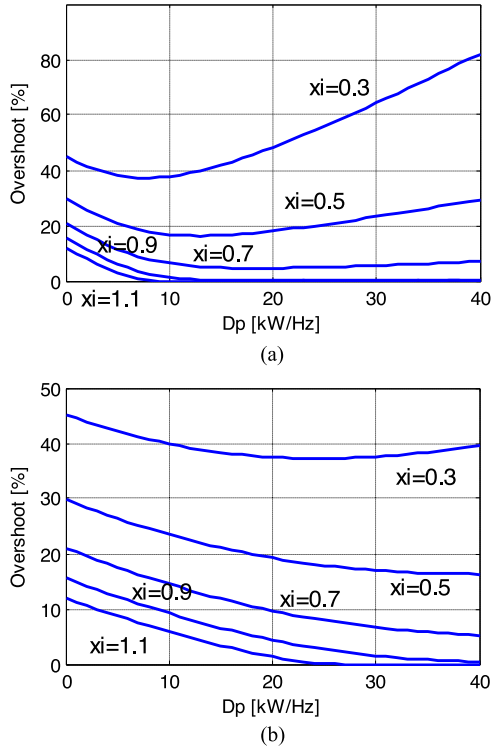

Fig. 6. The influence of the damping coefficient ξ on the overshoot of power step response: (a) $H = 2$ and (b) $H = 20$.

The analysis on the relation between ξ and the overshoot of the step response is shown in Fig. 6. Since the overshoot of the step response can considerably reflect the damping characteristics of the system, a value greater than 0.7 is proposed as the proper damping value, which can guarantee the overshoot of the step response to be smaller than 25%.

V. Simulation Results

Simulation studies are conducted for evaluating the performance of the proposed controller in cases of grid-connected converters connecting to weak (high-impedance) grids and island operations.

A. Performance When Interfacing Weak Grid

The influence of short circuit ratio (SCR) on the maximum power generation can be easily shown in (17), which defines the per-unit output power of a generation unit

$$P_{\mathrm{pu}} = SCR \cdot \sin\delta. \tag{17}$$

As seen from (17) the generated power will be always smaller than the rated power, when *SCR* equals to one (which yields an extremely weak grid).

The proposed control is able to inject relatively more power to weak grid under the variation of the power reference, compared

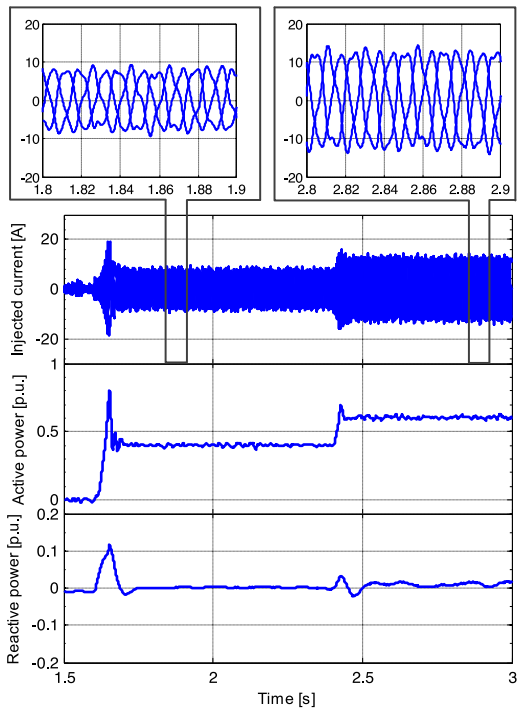

(a)

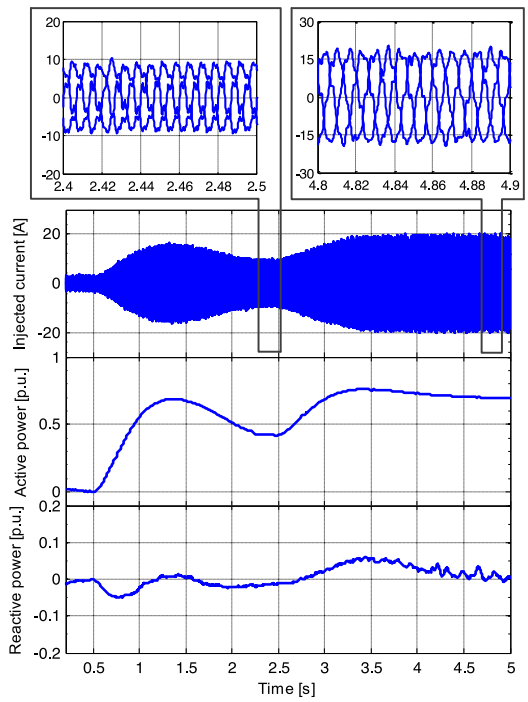

(b)

Fig. 7. Active power step response of the converter connected to weak grid: (a) conventional vector current control, (b) the proposed SPC.

with the conventional vector current control accompanied by PLL. This fact is validated in Fig. 7. In this case the SCR of the grid is configured to one.

Fig. 7(a) shows the case when the conventional vector current control is used, where the power injection can be achieved until 0.6 p.u. during steps of power reference based on the optimal

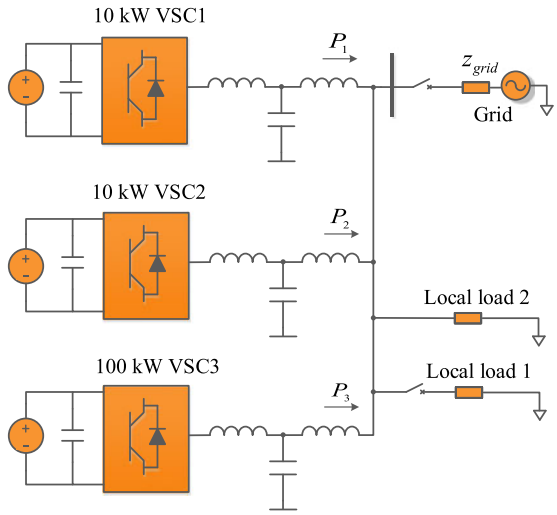

Fig. 8. A study case based on three paralleled grid-connected converters with different rated power.

tuning. When the proposed control is used, the power injection can be up to 0.7 p.u. as seen in Fig. 7(b).

Comparing the time response based on these two strategies, the latter one is featured by an inertial and more damped response in presence of power reference steps, which contributes in damping the transients.

B. Grid Disconnection and Island Operation

The proposed control is featured by the capability of feeding an island similar to synchronous machines. As mentioned before, the reference of reactive power is given by an outer *Q-V* droop controller.

Based on the control scheme in Fig. 1 aided by an outer *Q-V* droop controller, the island operation is possible. It is worth noting that the active power reference will not dominate the active power injection in island operation, instead, the power injection is determined by the virtual admittance and the *P-f* droop characteristics.

Fig. 8 shows a study case where a 100 kW and two 10 kW converters are connected to the grid in parallel, and serve local loads of 100 kW.

Based on (1), (2) and (12), the power variation of a generation unit can be expressed by,

$$\Delta P_{\mathrm{pu}} = \frac{1}{X_{\mathrm{pu}}} \Delta\delta. \tag{18}$$

According to (18), the virtual reactance for each converter is set to the same per-unit value for a proportional load sharing.

As an initial operation point, the grid connection switch is closed, and the power injection of 3 converters are 8 kW, 7 kW, and 70 kW, respectively, corresponding to 0.8 p.u., 0.7 p.u. and 0.7 p.u., and the local load is partly fed by the main grid.

Two events are considered in the case study. At 1.2 s, a failure in the main grid appears, while at 1.3 s, the step change of a local load takes place. Fig. 9 shows the results.

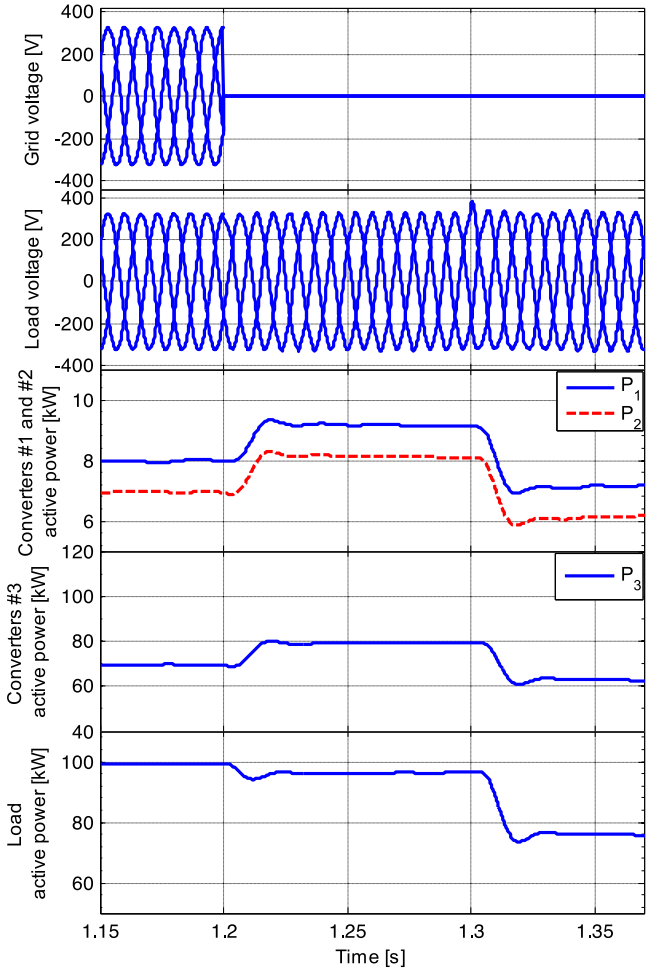

Fig. 9. The islanding action and load variations of a three-port system.

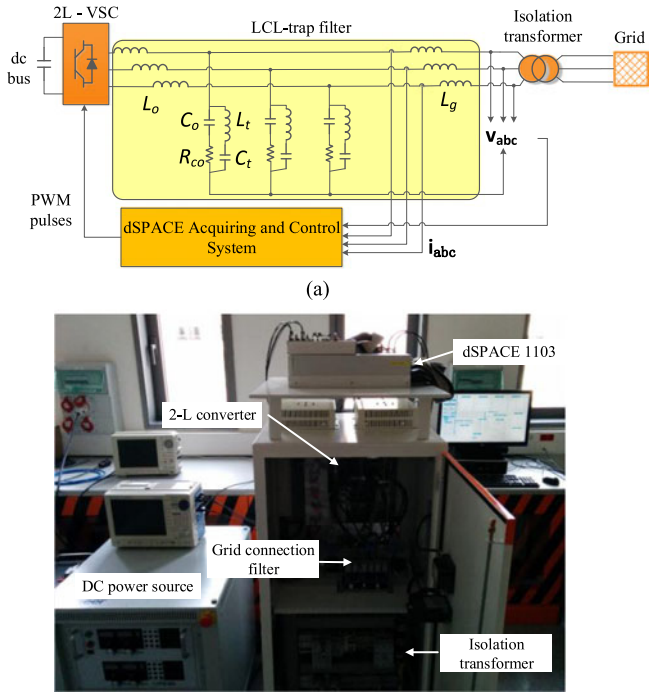

Fig. 10. 10 kW Experimental system: (a) setups configuration and scheme, (b) experimental setups.

TABLE I
KEY EXPERIMENTAL TESTS PARAMETERS

Symbol	Definition	Value
V_{DC}	dc-link voltage [V]	640
V_g	grid phase-to-phase voltage rms [V]	400
f_g	grid nominal frequency [Hz]	50
S_N	nominal power [kW]	10
f_{sw}	switching frequency [Hz]	10 050
ξ	damping coefficient [p.u.]	0.7
R	virtual resistance [p.u.]	0.1
X	virtual reactance [p.u.]	0.3

Regarding the first event, the local voltage is well maintained when the main grid failure occurs, thanks to the grid forming capability of the proposed control. The local voltage magnitude drop is calculated to be 4.22% as an acceptable value. As a response to this event, all the 3 converters increase the power injection, and the incremental power is all around 0.1 p.u. (with respect to the rated power of each converter). It complies with the designation of virtual reactance. The minor drop of the load power is due to the drop of the grid voltage magnitude.

During the second event, 20% of the local load (local load 1) is switched out. The local voltage is well maintained after a short transient, and all the converters decrease the power injection proportional to their rated power.

VI. EXPERIMENTAL RESULTS

An experimental system based on a 10 kW grid-connected converter is built to validate the proposed controller. The system structure is shown in Fig. 10(a), and a view of the setups is given in Fig. 10(b).

The dc bus is supplied by a 40 kW Magnapower dc power source, and the ac grid is formed by the California Instrument regenerative power source MX45. The control algorithm is implemented in a dSPACE 1103, and the parameters of the setups and the controller are shown in Table I.

For an easy evaluation and comparison of the experimental results, all the tests are done considering the same value of the damping coefficient ξ, which is fixed to 0.7. The virtual admittance is designed considering the range of the values of synchronous machines [18]. The per-unit value of virtual reactance is set to 0.3, corresponding to 15.3 mH, while the per-unit value of virtual resistance is set to 0.1 for sufficient damping, corresponding to 1.6 Ω.

Step changes of power reference and sweep of grid frequency are given to validate the dynamic performance of the proposed controller. The sweep of frequency is imposed by programming the power source with the frequency excursion that may occur in a grid with a limited amount of inertia.

For all the frequency sweep tests shown in this paper, the frequency changes as: it increases from 50 Hz to 49.9 Hz during 0.1 s, and then after 1 s, decreases to 50 Hz taking 0.1 s.

The CND controller is first implemented, and experimental results from two test cases are shown. In the first case, a step change in the active power reference from 5 kW to 10 kW is given when the controller is configured by $H = 10$ s and $D_P = 2$ kW/Hz. The injected current waveforms are shown in Fig. 11(a), where the injected active and reactive power calculated based on the experimental data are also plotted. The measured active and reactive power is processed by a low-pass filter to remove the high frequency noise without changing the outline. As shown in the results, the grid injected current and power change in a ramp instead of a sharp step, showing the inertia characteristics. The transient response without any oscillations also shows a proper damping of the system. And in the steady state, the injected active and reactive power is accurately controlled.

In the second case, grid frequency variation is given. The power reference is set to 6 kW and 0 kVar, and the controller has the same parameters as in the previous case. The results are shown in Fig. 11(b).

As seen from the results, the injected current and power oppose the variation of the grid frequency, showing a power synchronizing behavior. When the grid frequency decreases by 0.1 Hz, the active power stabilizes at 6.2 kW in steady state, complying with the designation of D_P (2 kW/Hz). The virtual synchronous frequency generated by the power loop also shows the inertia characteristics as well as an accurate lock of the grid frequency in steady state.

In contrast, the results from two cases when the MPL controller is used are shown in Fig. 12. H is designated the same value as the previous cases as $H = 10$ s.

Fig. 12(a) shows the response when a step in power reference is given. The MPL controller leads to a response with greater settling time and less overshoot.

Fig. 12(b) shows the response when variation in grid frequency is given. The variation of frequency is the same as the case when CND controller is used. The intrinsic droop characteristics are validated in Fig. 12(b). When the grid frequency changes from 50 to 49.9 Hz, the injected active power increases from 6 kW and stabilizes at 10 kW. The performance is coherent with the theoretical droop ratio, which is 40.522 kW/Hz. Then as long as the grid frequency deviates in 0.1 Hz, the power injection of the converter will change for 4 kW (0.4 p.u.), which could be much greater than the desired value. In order to adjust the droop ratio, the parameter ξ, H or X_{pu} has to be compromised.

The inertia dynamics given by the proposed CND controller is validated in experimental test and shown in Fig. 13. In this plot the power step responses under different H are shown.

Even if the time response will vary when different D_P is specified, which is seen by comparing Fig. 13(a) and (b), it can always be adjusted through adjusting the inertia constant H. Since the natural frequency ω_n is inversely proportional to the square root of the inertia constant H, the time of response is approximately proportional to the square root of H. In

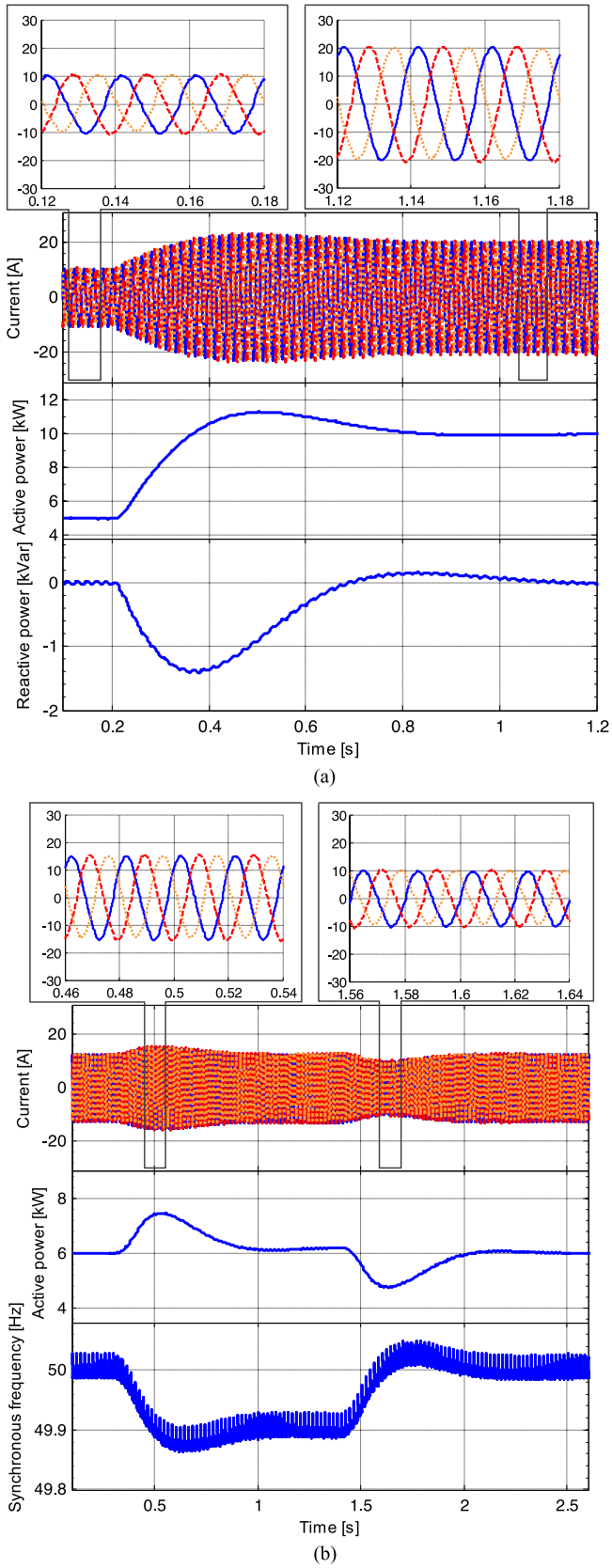

Fig. 11. Experimental results of the CND controller when $H = 10$ and $D_P = 2$: (a) a step in power reference, (b) response to grid frequency variations.

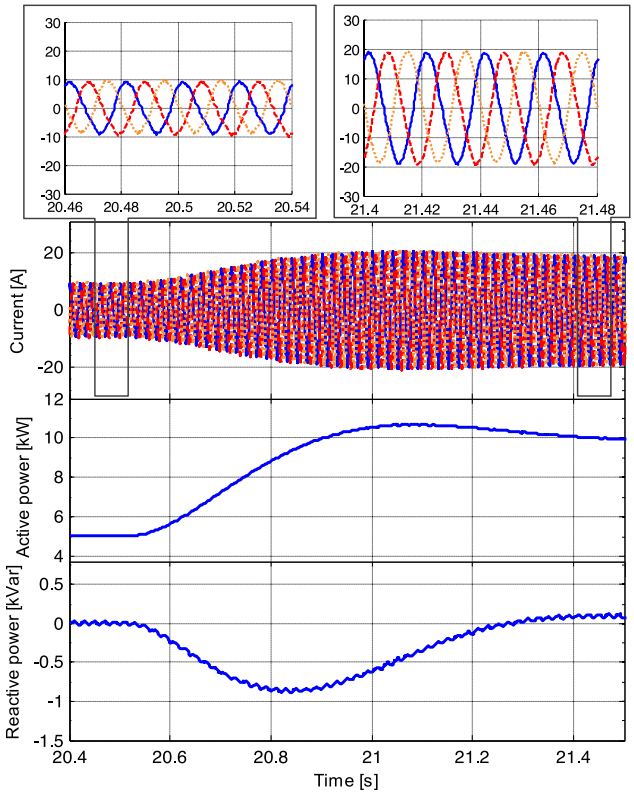

(a)

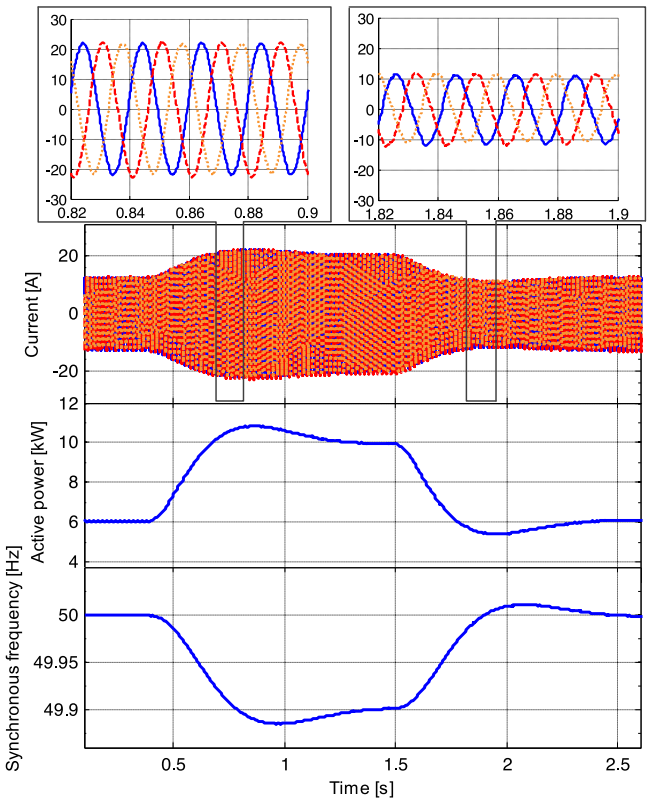

(b)

Fig. 12. Experimental results of the MPL controller when $H = 10$: (a) a step in power reference, (b) response to grid frequency variations.

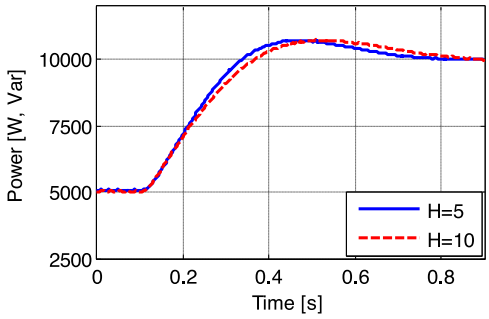

(a)

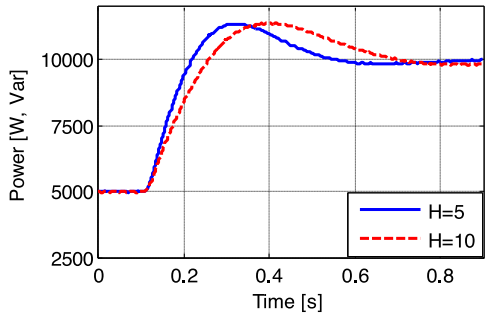

(b)

Fig. 13. Experimental responses to a step change in power reference from 5 kW to 10 kW: (a) $D_P = 20$ and (b) $D_P = 0$.

Fig. 13(a), the settling time of the two responses are calculated 544.1 ms and 732.4 ms, respectively. And in Fig. 13(b), are 479.0 ms and 677.5 ms, respectively.

In order to show the effect of the virtual admittance in grid voltage support, an unbalanced voltage dip is performed, in which the grid voltage in one phase is reduced by 30 V in rms. Fig. 14 shows the results based on the proposed controller. The unbalanced current can be explained by the reactive power injection in each phase, which is shown in Fig. 14(b). For phase A, where the voltage magnitude drops, the reactive power injection is significantly greater than the other two phases. It exhibits that the implemented virtual admittance can regulate the reactive power injection for each phase following the voltage magnitude. Therefore, the unbalance in grid voltage can be naturally diminished. It is worth noting that this feature of unbalanced voltage support cannot be achieved by an outer Q-V droop controller. Moreover, if a selective admittance for negative sequence is implemented, the level of unbalance can be further diminished.

Most of the inertia emulation control relies on the replication of the swing equations of synchronous machines, which is generalized as the MPL controller. Fig. 15 shows the power response to frequency variations of the proposed CND controller compared with the MPL controller based on the experimental data. D_P is specified to 0, 2 and 4 kW/Hz for the CND controller in three cases. For the MPL controller, D_P depends on H and ξ.

It can be seen in Fig. 15 that the steady state value of each response based on CND controller matches with its specification of D_P, showing the configurability of the droop ratio. In addition, the inertia and damping feature are also shown, where

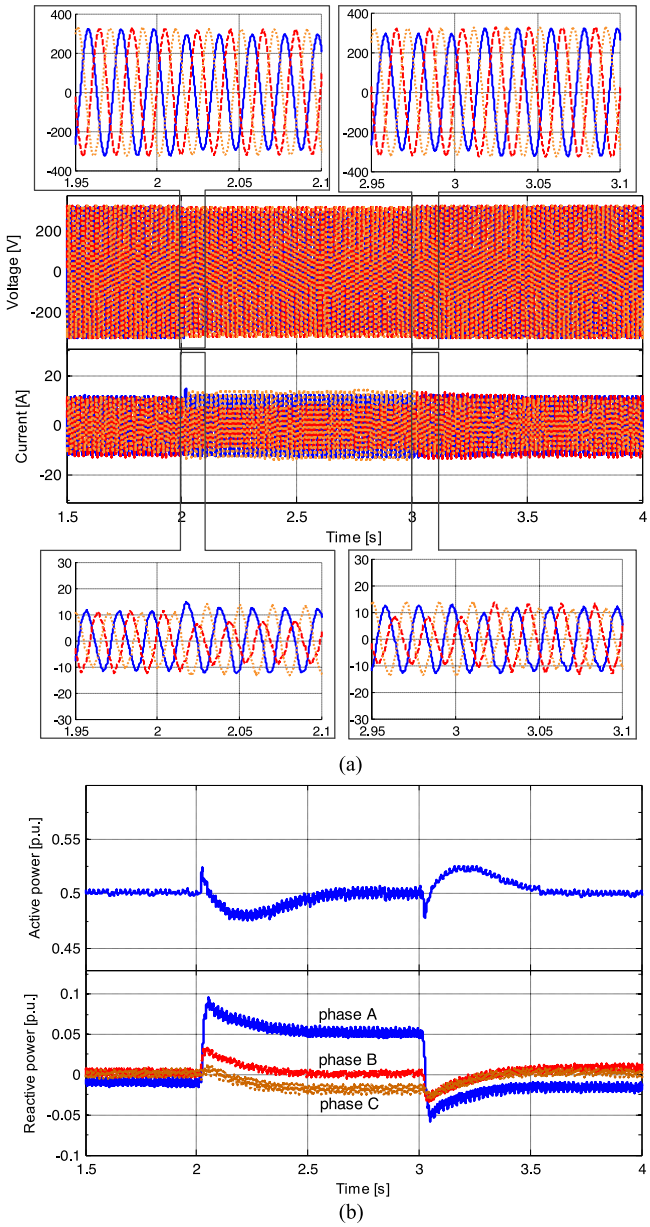

Fig. 14. Response in presence of unbalanced voltage dip: (a) voltage and current profiles, (b) active power and reactive power in each phase.

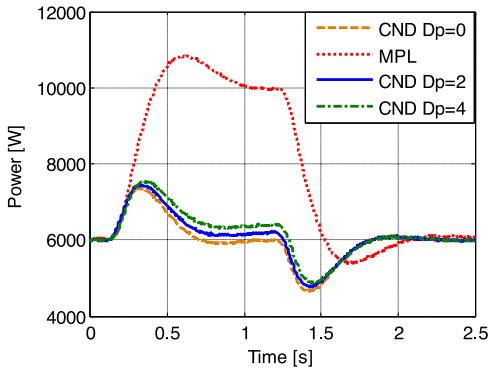

Fig. 15. Power responses to grid frequency variation based on the CND and MPL controller when $H = 10$.

the responses reach the steady state in hundreds of milliseconds without significant oscillations. The responses also show a behavior in opposing the grid frequency deviation. A stronger reaction occurs in the transient state than in the steady state. And in steady state it keeps supporting the grid according to the designation of the droop ratio D_P.

In contrast, the MPL controller exhibits a stronger droop effect that can be seen from the power change in Fig. 15. In a grid with low-inertia generation, the excursion of grid frequency can be as great as ± 2 Hz. Based on the droop slope of the MPL controller, the controlled converter could poses issues such as frequent saturation or low power quality injection. Therefore, an outer *P-f* droop controller has to be added to oppose the inherent droop, if the damping of the power loop is not reduced. However, it entails a more complex control design involving the use of a dedicated PLL, and the trade-off in designing the low-pass filter bandwidth.

VII. Conclusion

This paper proposed a synchronous power controller with inertia, damping and flexible droop characteristics for grid-connected power converters. The proposed controller shows more flexibility compared with the existing inertia emulation techniques, since it avoids the constraint between the damping and droop characteristics in the power regulating loop. Therefore, an outer *P-f* droop controller accompanied by a dedicated PLL is not needed for any operation stage, and the trade-off in designing the bandwidth of the droop loop low-pass filter is avoided. Besides, the fixed power control can be easily achieved in spite of grid frequency variations.

Experimental tests carried out on a two-level three-phase grid-connected converter have shown the good and expected performance of the proposed controller, which has been also endorsed by the simulation results.

References

[1] Q. C. Zhong and G. Weiss, "Static synchronous generators for distributed generation and renewable energy," in *Proc. Power Syst. Conf. Expo.*, 2009, pp. 1–6.

[2] K. De Brabandere, B. Bolsens, J. Van Den Keybus, A. Woyte, J. Driesen, and R. Belmans, "A voltage and frequency droop control method for parallel inverters," *IEEE Trans. Power Electron.*, vol. 22, no. 4, pp. 1107–1115, Jul. 2007.

[3] J. M. Guerrero, J. C. Vasquez, J. Matas, L. G. De Vicuña, and M. Castilla, "Hierarchical control of droop-controlled AC and DC microgrids—A general approach toward standardization," *IEEE Trans. Ind. Electron.*, vol. 58, no. 1, pp. 158–172, Jan. 2011.

[4] T. Loix, K. De Brabandere, J. Driesen, and R. Belmans, "A three-phase voltage and frequency droop control scheme for parallel inverters," in *Proc. IEEE Ind. Electron. Conf.*, 2007, pp. 1662–1667.

[5] J. Rocabert, A. Luna, F. Blaabjerg, and P. Rodri´ guez, "Control of power converters in AC microgrids," *IEEE Trans. Power Electron.*, vol. 27, no. 11, pp. 4734–4749, Nov. 2012.

[6] K. Rouzbehi, A. Miranian, A. Luna, and P. Rodriguez, "A generalized voltage droop strategy for control of multi-terminal DC grids," *IEEE Trans. Ind. Appl.*, vol. 51, no. 1, pp. 59–64, Jan./Feb. 2013.

[7] H. P. Beck and R. Hesse, "Virtual synchronous machine," in *Proc. Int. Conf. Elect. Power Quality Utilisation*, 2007, pp. 1–6.

[8] L. Zhang, L. Harnefors, and H. P. Nee, "Power-synchronization control of grid-connected voltage-source converters," *IEEE Trans. Power Syst.*, vol. 25, no. 2, pp. 809–820, May 2010.

[9] M. P. N. Van Wesenbeeck, S. W. H. De Haan, P. Varela, and K. Visscher, "Grid tied converter with virtual kinetic storage," in *Proc. IEEE Bucharest PowerTech*, 2009, no. 1, pp. 1–7.
[10] H. Alatrash, A. Mensah, E. Mark, G. Haddad, and J. Enslin, "Generator emulation controls for photovoltaic inverters," *IEEE Trans. Smart Grid*, vol. 3, no. 2, pp. 996–1011, Jun. 2012.
[11] M. A. Torres, L. A. Lopes, L. A. Moran, and J. R. Espinoza, "Self-tuning virtual synchronous machine: A control strategy for energy storage systems to support dynamic frequency control," *IEEE Trans. Energy Convers.*, vol. 29, no. 4, pp. 833–840, Dec. 2014.
[12] L. Zhang, L. Harnefors, and H. P. Nee, "Interconnection of two very weak AC systems by VSC-HVDC links using power-synchronization control," *IEEE Trans. Power Syst.*, vol. 26, no. 1, pp. 344–355, Feb. 2011.
[13] Q. C. Zhong, P. Nguyen, Z. Ma, and W. Sheng, "Self-synchronized synchronverters: Inverters without a dedicated synchronization unit," *IEEE Trans. Power Electron.*, vol. 29, no. 2, pp. 617–630, Feb. 2014.
[14] Q. C. Zhong and G. Weiss, "United States Patent Application Publication: Static Synchronous Generators," US 2011/0270463 A1, 2011.
[15] Q. C. Zhong and G. Weiss, "Synchronverters: Inverters that mimic synchronous generators," *IEEE Trans. Ind. Electron.*, vol. 58, no. 4, pp. 1259–1267, Apr. 2011.
[16] S. M. Ashabani and Y. A. R. I. Mohamed, "A flexible control strategy for grid-connected and islanded microgrids with enhanced stability using nonlinear microgrid stabilizer," *IEEE Trans. Smart Grid*, vol. 3, no. 3, pp. 1291–1301, Sep. 2012.
[17] P. Rodriguez, I. Candela, J. Rocabert, and R. Teodorescu, "European patent application: Virtual controller of electromechanical characteristics for static power converters," WO 2012/117132, 2014.
[18] P. Rodriguez, I. Candela, C. Citro, J. Rocabert, and A. Luna, "Control of grid-connected power converters based on a virtual admittance control loop," in *Proc. Eur. Conf. Power Electron. Appl.*, 2013, pp. 1–10.
[19] P. Rodriguez, I. Candela, and A. Luna, "Control of PV generation systems using the synchronous power controller," in *Proc. Energy Convers. Congr. Expo.*, 2013, pp. 993–998.
[20] S. D. Arco and J. A. Suul, "Virtual synchronous machines—Classification of implementations and analysis of equivalence to droop controllers for microgrids," in *Proc. PowerTech*, 2013, pp. 1–7.
[21] S. D. Arco and J. A. Suul, "Equivalence of virtual synchronous machines and frequency-droops for converter-based microgrids," *IEEE Trans. Smart Grid*, vol. 5, no. 1, pp. 394–395, Jan. 2014.
[22] P. Rodriguez, I. Candela, J. Rocabert, and R. Teodorescu, "United States Patent Application Publication: Synchronous power controller for a generating system based on static power converters," 2014.
[23] P. Rodriguez, I. Candela, J. Rocabert, and R. Teodorescu, "United States Patent Application Publication: Virtual admittance controller based on static power converters," US 2014/0049233 A1, 2014.
[24] P. Kundur, *Power System Stability and Control*. New York, NY, USA: McGraw-Hill, 1994.
[25] J. Duncan Glover, M. S. Sarma, and T. J. Overbye, *Power system analysis and design*, 4th ed. Boston, MA, USA: Cengage Learning, 2010.

Weiyi Zhang (S'15) received the B.Eng. degree in electrical engineering and the M.Sc. degree in power electronics and electrical drive from Northwestern Polytechnical University, Xi'an, China, in 2010 and 2013, respectively. He has been working toward the Ph.D. degree at the Research Center on Renewable Electrical Energy Systems in Technical University of Catalonia, Barcelona, Spain, since 2013. His current research interests include control of power converters and integration of distributed generation systems.

Antoni Mir Cantarellas (S'12) received the B.Sc. degree in electrical engineering from the Technical University of Catalonia (UPC), Barcelona, Spain, and the M.Sc. degree in wind power systems from Aalborg University, Aalborg, Denmark, in 2010 and 2012, respectively. He is currently working toward the Ph.D. degree from the UPC.

In 2012, he joined Abengoa Research, Abengoa, Seville, where he is currently a Ph.D. Fellow in the area of distributed generation. His current research interests include distributed generation and control of power plants.

Joan Rocabert (S'08–M'11) was born in Barcelona, Spain. He received the M.Sc. degree in electrical engineering in 2003 and the Ph.D. degree in electrical engineering on the topic of PV microgrids control in 2010 both from the Technical University of Catalonia, Barcelona, Spain, in 2010.

From 2004 to 2008, he was a Research Assistant at the Department of Electronic Engineering, Technical University of Catalonia. Since 2008, he has been with the Department of Electrical Engineering, working as a Researcher and Assistant Professor. His current research interests include integration of distributed generation, energy storage systems, and power electronics applied to photovoltaic and wind energy systems, particularly their application into microgrids.

Alvaro Luna (S'07–M'10) received the B.Sc., M.Sc., and Ph.D. degrees from the Technical University of Catalonia (UPC), Barcelona, Spain, in 2001, 2005, and 2009, respectively, all in electrical engineering. He joined as a Faculty Member at UPC in 2005, where he is currently an Assistant Professor. His research interests include wind turbines control, PV systems, integration of distributed generation, and power conditioning.

Pedro Rodriguez (S'99–M'04–SM'10–F'13) received the M.Sc. and Ph.D. degrees in electrical engineering from the Technical University of Catalonia (UPC), Barcelona, Spain, in 1994 and 2004, respectively. He was a Postdoctoral Researcher at the Center for Power Electronics Systems, Virginia Tech, Blacksburg, in 2005, and at the Department of Energy Technology, Aalborg University (AAU), in 2006. He joined the Faculty of UPC as an Assistant Professor in 1990, where he became the Director of the Research Center on Renewable Electrical Energy Systems at the Department of Electrical Engineering. He was also a Visiting Professor at the AAU from 2007 to 2011, acting as a Cosupervisor of the Vestas Power Program. He still lectures Ph.D. courses at the AAU every year. Since 2011, he has been the Head of Electrical Engineering Division in Abengoa Research, although he is still joined to the UPC as a Part Time Professor. He has coauthored one book and more than 100 papers in technical journals and conference proceedings. He is the holder of seven licensed patents. His research interests include integration of distributed generation systems, smart grids, and design and control of power converters.

Dr. Rodriguez is a member of the administrate committee of the IEEE Industrial Electronics Society (IES), the General Chair of IEEE-IES Gold and Student Activities, the Vice Chair of the Sustainability and Renewable Energy Committee of the IEEE Industry Application Society, and a member of the IEEE-IES Technical Committee on Renewable Energy Systems. He is an Associate Editor of the IEEE TRANSACTION ON POWER ELECTRONICS.